A Two-Scale Scattering Model for Foam-Free Sea Microwave Brightness Temperatures

FRANK J. WENTZ

F. J. Wentz & Associates, Box 162, M.I.T. Branch P.O., Cambridge, Massachusetts 02139

A two-scale surface comprised of small irregularities superimposed on large undulations is defined from an empirical sea spectrum. The scattering of microwave radiation from the surface is modeled by combining geometric-optics and small-scale perturbation theory in a manner consistent with the conservation of energy. The two-scale scattering model includes multiple reflections and shadowing effects. Foam-free sea brightness temperatures are computed and show that the presence of small-scale roughness increases the brightness temperature at nadir. Comparisons with experimental data show better agreement for the two-scale model than for the geometric-optics model. Changing the small-scale perturbation parameter from 0.125 to 0.25 slightly affects the computed brightness temperatures.

INTRODUCTION

The potential of microwave radiometry to sense sea surface temperature and roughness has generated interest in theoretical models for sea brightness temperatures. Brightness temperature measurements that excluded foam [*Hollinger*, 1970, 1971; *Van Melle et al.*, 1973] disagreed with *Stogryn*'s [1967] geometric-optics model. *Strong* [1971] suggested that the discrepancy resulted from the neglect by Stogryn's model of surface irregularities that are small in comparison to the radiation wavelength. *Wu and Fung* [1972] took into account the small-scale sea roughness by extending *Semyonov*'s [1966] two-scale scattering theory to compute surface emission, but the wind dependence of the Wu and Fung model was difficult to assess because the small-scale rms height was derived in an a posteriori manner by fitting theoretical computations to experimental data.

In this paper the two-scale scattering model is improved upon by including shadowing and multiple reflections and by combining the large- and small-scale scattering in a manner consistent with the conservation of energy. The statistical sea roughness parameters are derived from an empirical sea spectrum [*Pierson and Stacy*, 1973], and the computed sea brightness temperatures are compared with experimental data [*Hollinger*, 1971].

SEA BRIGHTNESS TEMPERATURE MODEL

The inputs for the sea brightness temperature model are the small-scale perturbation parameter, the observational parameters, and the environmental parameters. The observational parameters are the following: (1) the frequency f of the observed radiation, (2) the electric field $\hat{E}_0$ of the observed radiation, and (3) the incidence angle θ made by $-\hat{k}_0$ and $\hat{z}$, where $-\hat{k}_0$ is the unit propagation vector of the observed radiation and $\hat{z}$ is the unit normal to the mean scattering surface. The environmental parameters are the following: (1) the seawater temperature T_w, (2) the seawater salinity s, (3) the wind friction velocity U_*, (4) the wind direction $\hat{u}$, and (5) the downward sky brightness temperature $T_d(\theta_s)$, which is a function of the zenith sky angle θ_s. $T_d(\theta_s)$ is assumed to be independent of azimuth angle.

The two-scale zenith scattering coefficients $\Gamma(\theta_s, \theta)$ can be computed once all these parameters are assigned values. $\Gamma(\theta_s, \theta)$ is defined by

$$\Gamma(\theta_s, \theta) = \int_{-\pi}^{\pi} d\phi_s \Gamma(\theta_s, \phi_s, \theta) \tag{1}$$

where θ_s and ϕ_s are the zenith and azimuth angles specifying the direction of scattering and $\Gamma(\theta_s, \phi_s, \theta)$ are the differential scattering coefficients defined by *Peake* [1959]. The surface emissivity $\xi(\theta)$ is given by

$$\xi(\theta) = 1 - \int_0^{\pi/2} d\theta_s \sin \theta_s \Gamma(\theta_s, \theta) \tag{2}$$

and the brightness temperature at the sea surface is given by

$$T_B(\theta) = \xi(\theta) T_w + \int_0^{\pi/2} d\theta_s \sin \theta_s \Gamma(\theta_s, \theta) T_d(\theta_s) \tag{3}$$

where the first term is the surface emission and the second term is the scattered sky radiation.

Semyonov's [1966] two-scale scattering theory assumes that the scattering surface Σ comprises a small-scale surface Σ_s superimposed onto a large-scale surface Σ_l. The rms height ζ of Σ_s is assumed to be small in comparison to the radiation wavelength λ, and the rms slope of Σ_s is assumed to be small in comparison to unity. These two restrictions allow for the application of perturbation theory [*Rice*, 1951] in treating the radiation scattered from Σ_s. The radius of curvature at all points on Σ_l is assumed to be large in comparison to λ. This restriction is necessary for the validity of the following approximation, which is an extension of the tangent plane approximation. The field at any point on Σ is approximated by the field that would be present on the plane tangent to Σ_l at that point, Σ_s being superimposed on the tangent plane.

Surfaces Σ_s and Σ_l are described by the roughness spectra $W_s(K, \phi)$ and $W_l(K, \phi)$, respectively:

$$\begin{aligned} W_s(K, \phi) &= W(K, \phi) \qquad K > K_c \\ W_s(K, \phi) &= 0 \qquad K \le K_c \end{aligned} \tag{4}$$

$$\begin{aligned} W_l(K, \phi) &= 0 \qquad K > K_c \\ W_l(K, \phi) &= W(K, \phi) \qquad K \le K_c \end{aligned} \tag{5}$$

where $W(K, \phi)$ is the roughness spectrum of the surface Σ, K denotes the radial wave number, and ϕ denotes the polar angle measured from the upwind direction. The assignment of a value to the cutoff wave number K_c will be discussed below. The large-scale sea surface consists of all sea waves with wave numbers less than or equal to K_c, and the small-scale sea surface consists of all sea waves with wave numbers greater than K_c. *Pierson and Stacy*'s [1973] empirically derived directional spectrum $S(K, \phi)$ for a fully developed sea is used for computing brightness temperatures. The relationship between $W(K, \phi)$ and $S(K, \phi)$ is

$$W(K, \phi) = (2/K)[S(K, \phi) + S(K, \phi + \pi)] \tag{6}$$

The amplitude of $S(K, \phi)$ is a function of the friction velocity U_*. The isotropic form of the sea spectrum is assumed for wave numbers greater than K_c.

The value of the cutoff wave number K_c is determined by assigning a value to the small-scale perturbation parameter $k\zeta$, where k is the radiation wave number equaling $2\pi/\lambda$. Perturbation theory requires that $k\zeta$ be small in comparison to unity. The small-scale height variance is given by

$$\zeta^2 = \tfrac{1}{4} \int_{K_c}^{\infty} dKK \int_{-\pi}^{\pi} d\phi\, W(K, \phi) \tag{7}$$

where the lower limit K_c follows from (4). The above integral can be evaluated in closed form, ζ being expressed as a function of K_c and U_*. Then K_c can be solved for in terms of ζ and U_*. Three values for $k\zeta$, 0, 0.125, and 0.25, are considered in the brightness temperature computations. The corresponding values of K_c for each radiation frequency and friction velocity to be considered are given in Table 1. When $k\zeta = 0$, K_c goes to infinity, and no small-scale roughness is present. For this case, scattering from Σ is described by geometric-optics. The large-scale slope variances σ_u^2 and σ_c^2 in the upwind and crosswind directions are computed from

$$\sigma_m^2 = \tfrac{1}{4} \int_0^{K_c} dKK^3 \int_{-\pi}^{\pi} d\phi \Psi_m W(K, \phi) \tag{8}$$

where $m = u$ or c, $\Psi_u = \cos^2 \phi$, and $\Psi_c = \sin^2 \phi$. Values for the large-scale slope variance $\sigma^2 = \sigma_u^2 + \sigma_c^2$ for each radiation frequency and friction velocity to be considered are given in Table 2. When $k\zeta = 0$, σ^2 is the slope variance of the overall sea surface and is independent of the radiation frequency. For this case the values of σ^2 for the three friction velocities 20.2, 34.6, and 50.2 cm/s are 0.061, 0.094, and 0.142, respectively.

The scattering coefficients $\Gamma(\theta_s, \theta)$ are found by representing the radiation incident onto Σ as a large set of parallel propagation vectors $\hat{k}_0$ having an electric field $\hat{E}_0$. Each $\hat{k}_0$ is treated separately according to the following procedure. The normal $\hat{\eta}$ to Σ_l at the point where $\hat{k}_0$ intersects is found by taking a random sample from the set $\{\hat{\eta}\}$ of surface normals defined in Appendix A. As is shown in Figure 1, the incident radiation produces coherent reflected power having a propagation vector $\hat{k}_r$ and incoherent scattered power that propagates in all directions. The reflected power divided by the incident power is given by the squared magnitude $|\mathbf{E}_r|^2$ of the reflected electric field $\mathbf{E}_r$. The power scattered between zenith angles θ_s and $\theta_s + d\theta_s$ divided by the incident power is given by $\gamma(\theta_s, \hat{k}_0, \hat{\eta}) \sin \theta_s\, d\theta_s$, where $\gamma(\theta_s, \hat{k}_0, \hat{\eta})$ are the small-scale zenith scattering coefficients. Expressions for $\hat{k}_r$, $|\mathbf{E}_r|^2$, and $\gamma(\theta_s, \hat{k}_0, \hat{\eta})$ appear in Appendix B. In the brightness temperature computations, 100 zenith angles are considered with $\sin \theta_s\, d\theta_s = 0.01$. All the scattered power is assumed to escape the surface without secondary intersections occurring. The probability that $\hat{k}_r$ escapes the surface is taken to be the shadowing probability $\Lambda(-\hat{k}_r, \hat{\eta})$ that an incident propagation vector $-\hat{k}_r$ is not shadowed by a remote portion of the surface from the point where $\hat{k}_0$ intersects. Parameter $\Lambda(-\hat{k}_r, \hat{\eta})$ is derived in Appendix A. A random number on the interval 0–1 is generated and is compared with $\Lambda(-\hat{k}_r, \hat{\eta})$. If the random number is less than $\Lambda(-\hat{k}_r, \hat{\eta})$, $\hat{k}_r$ is assumed to escape. Otherwise, $\hat{k}_r$ intersects the surface at another point, as is shown in Figure 1. For this second intersection, $\hat{k}_r$ is considered to be the incident propagation vector, $\mathbf{E}_r$ becomes the incident field, and another surface normal $\hat{\eta}$ is generated. The small-scale zenith scattering coefficients for this second intersection are added to the $\gamma(\theta_s, \hat{k}_0, \hat{\eta})$ that were computed for the initial intersection, and a new reflected propagation vector $\hat{k}_r$ and field $\mathbf{E}_r$ are found. This procedure continues until $\hat{k}_r$ escapes, and then the escaping reflected power is added to the power that has been scattered between θ_r and $\theta_r + d\theta_r$, where θ_r is the zenith angle of the escaping $\hat{k}_r$. That is to say, $|\mathbf{E}_r|^2$ is added to $\gamma(\theta_r, \hat{k}_0, \hat{\eta}) \sin \theta_r\, d\theta_r$.

A total number of N incident propagation vectors are considered, and N corresponding sets of 100 scattering coefficients $\gamma(\theta_s, \hat{k}_0, \hat{\eta})$ are computed as described above. The two-scale zenith scattering coefficients $\Gamma(\theta_s, \theta)$ are taken to be

$$\Gamma(\theta_s, \theta) = \langle \gamma(\theta_s, \hat{k}_0, \hat{\eta}) \rangle \tag{9}$$

where angle brackets denote the average of the N sets. In general, $N = 10^4$ results in a sampling error of less than 0.5°K in terms of brightness temperature. This treatment of scattering conserves energy exactly because at each surface intersection the sum of the reflected and scattered power equals the incident power for a perfectly conducting surface, as is shown in Appendix B.

COMPARISON WITH EXPERIMENT

Hollinger [1971] measured sea brightness temperatures from Argus Island tower. During data analysis the relatively high brightness temperature of sea foam was readily recognized and

TABLE 1. Cutoff Sea Wave Number

U_*, cm/s	Cutoff Sea Wave Number K_c, cm^{-1}, $k\zeta = 0.125$, 1.41 GHz	8.36 GHz	19.3 GHz	$k\zeta = 0.25$, 1.41 GHz	8.36 GHz	19.3 GHz
20.2	0.12	1.2	2.6	0.055	0.54	1.3
34.6	0.17	1.4	3.2	0.069	0.70	1.6
50.2	0.22	1.7	3.8	0.089	0.87	2.0

TABLE 2. Large-Scale Slope Variance

U_*, cm/s	Large-Scale Slope Variance σ^2, $k\zeta = 0.125$, 1.41 GHz	8.36 GHz	19.3 GHz	$k\zeta = 0.25$, 1.41 GHz	8.36 GHz	19.3 GHz
20.2	0.015	0.033	0.044	0.012	0.024	0.035
34.6	0.022	0.054	0.070	0.016	0.039	0.056
50.2	0.032	0.081	0.106	0.022	0.060	0.085

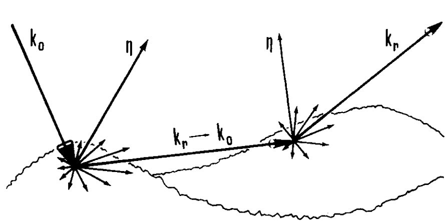

Fig. 1. A double reflection from a two-scale surface, where the small arrows represent the scattered radiation.

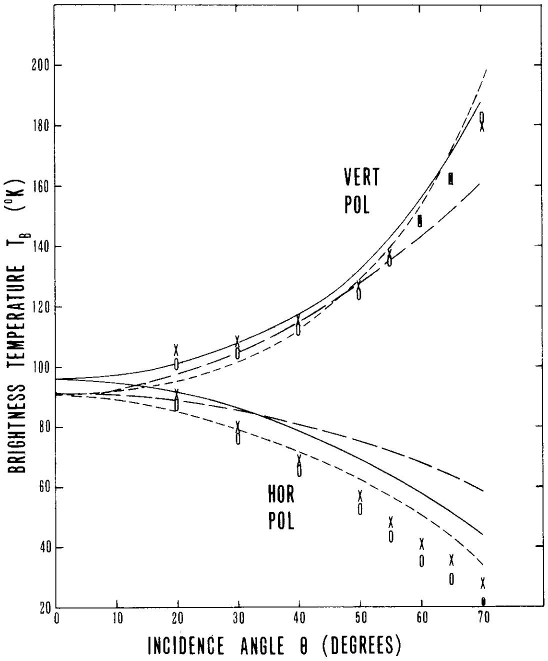

Fig. 2. Comparison of computed and experimental brightness temperatures for f = 1.41 GHz, ϵ = 71.5 − 69.3j, and τ = 0.009 Np. The large-dashed and solid curves show the large-scale geometric-optics and the two-scale computations, respectively, for a 13.5 m/s wind speed. The small-dashed curves show the specular computations. The circles and crosses are the average measurements for wind speeds of 0.5 and 13.5 m/s, respectively.

was excluded from the averaged antenna temperatures. A first-order correction for atmospheric effects was made by subtracting the specular reflection of the downward sky radiation $T_d(\theta)$ from the measured brightness temperature $T_B(\theta)$, and the atmospheric-corrected brightness temperature denoted simply as T_B is

$$T_B = T_B(\theta) - [1 - \xi_{sp}(\theta)]T_d(\theta) \qquad (10)$$

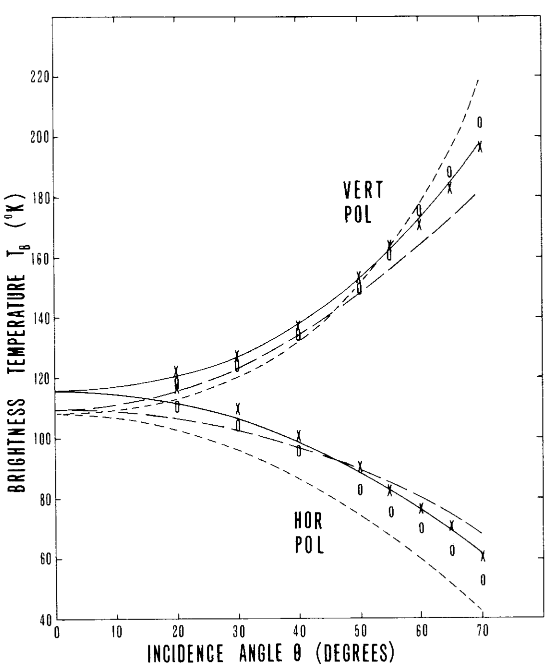

Fig. 3. Same as Figure 2 except f = 8.36 GHz, ϵ = 58.5 − 36.8j, and τ = 0.017 Np.

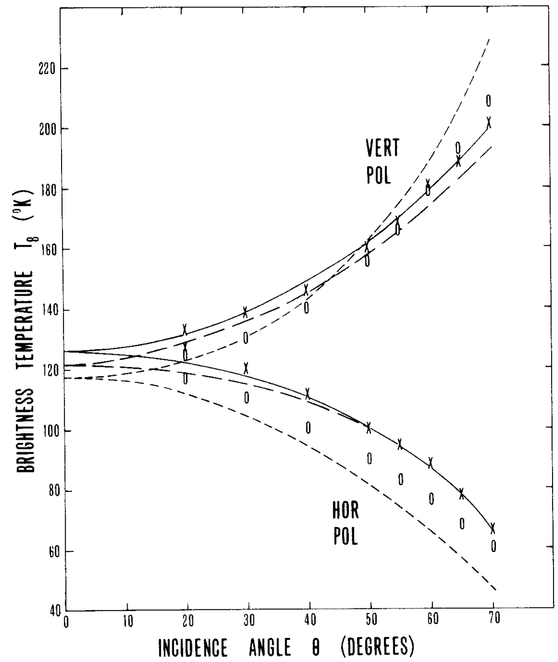

Fig. 4. Same as Figure 2 except f = 19.3 GHz, ϵ = 34.8 − 37.1j, and τ = 0.069 Np.

where $T_B(\theta)$ is defined by (3) and $\xi_{sp}(\theta)$ is the emissivity for a specular sea surface. $T_d(\theta)$ is taken to be

$$T_d(\theta) = T_a\{1 - \exp[-\tau\Xi(\theta)]\} \qquad (11)$$

where $\Xi(\theta)$ is the air mass function [*Allen,* 1963]. The atmospheric opacity τ and air temperature T_a were measured by Hollinger.

Brightness temperatures are computed for three frequencies, 1.41, 8.36, and 19.3 GHz, and for four wind speeds, 0, 6.5, 10.0, and 13.5 m/s. The sea water permittivities ϵ at the three frequencies are computed from expressions given by *Porter and Wentz* [1971] assuming a water temperature T_w equaling 291°K and a salinity s equaling 35‰, which are the average values reported by Hollinger. The friction velocities U_* that appear in Table 1 correspond to the three nonzero wind speeds and are computed from expressions given by *Cardone* [1969]. Hollinger's anemometer height of 43 m is used in the U_* computations, and the air-sea temperature difference $T_a - T_w$ is assumed to be zero. The T_B observations are assumed to be in the upwind direction. A specular surface is assumed for the zero wind speed case.

In Figures 2–4 the vertical and horizontal polarization components of Hollinger's T_B measurements are plotted versus incidence angle θ for the above three frequencies and for two wind speeds, 0.5 and 13.5 m/s. These measurements are an average over varying wind directions and air-sea temperature differences. Also shown are the computed T_B for a two-scale surface with U_* = 50.2 cm/s and $k\zeta$ = 0.25, for a large-scale surface with U_* = 50.2 cm/s and $k\zeta$ = 0, and for a specular surface. The T_B computations for $k\zeta$ = 0.125, which are not shown, are only slightly different from the computations for $k\zeta$ = 0.25. At nadir the two-scale T_B is higher than the large-scale geometric-optics T_B owing to the inclusion of small-scale roughness. In consideration of the 5–10% reported absolute error in measurement the agreement between the two-scale T_B and measurements is surprisingly good at the two higher frequencies. The large discrepancy at 1.41 GHz is possibly due to absolute calibration errors (J. P. Hollinger, private communication, 1974). In all cases the dependence of the two-scale T_B on θ is more in accord with the experimental data than the dependence shown by the geometric-optics T_B is. The difference between the two-scale T_B and the geometric-optics T_B is greatest at 1.41 GHz because a substantial portion of the sea spectrum satisfies the small-scale roughness criterion of $K > K_c$ at this lowest frequency. The poor agreement between the measurements for a 0.5 m/s wind and the specular T_B is probably due in part to the presence of swells. Also an inadequate antenna pattern correction technique could contribute to the disagreement.

To investigate the T_B wind dependence in greater detail, Hollinger found linear least squares fits for the T_B data as a function of wind speed U. The slopes $\Delta T_B/\Delta U$ of these fits for horizontal and vertical polarizations were reported along with the slopes $\Delta p/\Delta U$, where p denotes the percentage polarization defined as the ratio of the difference between the horizontal and vertical T_B components to the sum. In Figures 5–7 the experimental values of these three slopes are plotted versus θ for the three frequencies. Also shown are the slopes computed from the two-scale model, with $k\zeta = 0.125$ and 0.25, and from the geometric-optics model, with $k\zeta = 0$. These values are obtained by finding the linear least squares fits for the T_B computations at the above four wind speeds. Compared to the geometric-optics model, the two-scale model shows a larger wind dependence at nadir and a smaller dependence at the large incidence angles. The small wind dependence at nadir shown by the geometric-optics model is almost completely due to the downward sky radiation that is scattered, rather than reflected, from the sea surface. For vertical polarization the geometric-optics model shows a wind speed independence near $\theta = 50°$. In comparison, the two-scale model agrees better with the experimental data by showing a wind speed independence between 53° and 63° depending on frequency. The major disagreement between the two-scale computations and the measurements is seen at 8.36 and 19.3 GHz for large θ. Better agreement would be achieved if the large-scale slope variance σ^2 calculated from the Pierson and Stacy sea spectrum were reduced by about $1/4$. In view of this, the disagreement may be due to the incomplete development of the observed sea states. Also *Pierson and Stacy* [1973] reported that their sea slope variance was at least a factor of 2 higher than that reported by *Cox and Munk* [1954].

CONCLUSIONS

In comparison with the geometric-optics model, the two-scale scattering model shows better agreement with sea brightness temperature measurements in that the two-scale model more accurately predicts the dependence of brightness temperature on incidence angle and wind speed. At nadir the presence of small-scale roughness increases the brightness temperature. A variation in the small-scale perturbation parameter from 0.125 to 0.25 slightly affects the computed brightness temperatures. The largest difference between the geometric-optics and the two-scale computations occurs at 1.41 GHz because at this lowest frequency a substantial portion of the sea spectrum satisfies the small-scale roughness criterion. Some disagreement between the wind dependence of the two-scale brightness temperatures and the experimental data occurs at the large incidence angles and may be due to the incomplete development of the observed sea states.

APPENDIX A: THE SURFACE NORMAL SET

The set $\{\hat{\eta}\}$ of surface normals is defined as the set of random deviates having the probability density function $P(\hat{\eta}|\hat{k}_0)$. $P(\hat{\eta}|\hat{k}_0)\,d\eta_1\,d\eta_2$ is the conditional probability that a differential portion dS of the large-scale surface Σ_l has a unit normal lying between $\hat{\eta}$ and $\hat{\eta} + d\hat{\eta}$, given the condition that the incident propagation vector $\hat{k}_0$ intersects dS. The components of $\hat{\eta}$ are denoted by η_1, η_2, and η_3, and the differential components of $d\hat{\eta}$

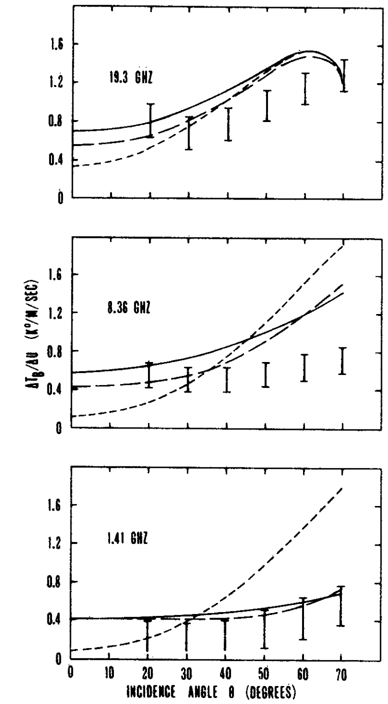

Fig. 5. Comparison of computed and experimental derivatives of brightness temperature with respect to wind speed for horizontal polarization. The solid and large-dashed curves show the two-scale computations for $k\zeta = 0.25$ and 0.125, respectively. The small-dashed curves show the large-scale geometric-optics computations. The experimental values are shown by the error bars.

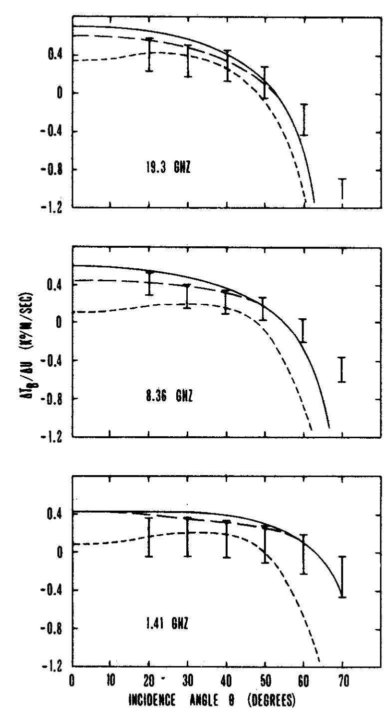

Fig. 6. Same as Figure 5 except that the derivatives for vertical polarization are shown.

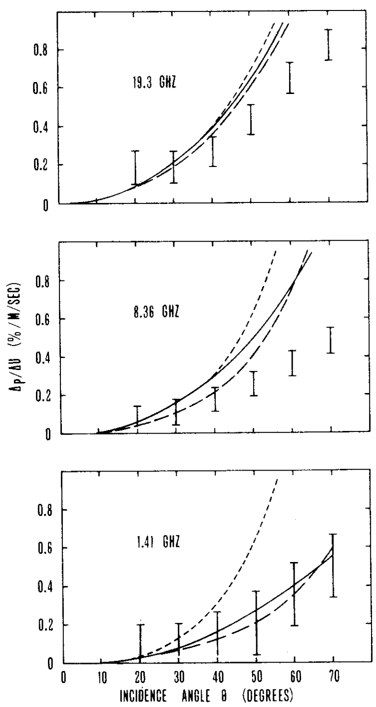

Fig. 7. Same as Figure 5 except that the derivatives for percentage polarization are shown.

are denoted by $d\eta_1$, $d\eta_2$, and $d\eta_3$. Requiring that the surface normal has unit magnitude results in $d\eta_3$ being a dependent variable of $\hat{\eta}$, $d\eta_1$, and $d\eta_2$. Once $P(\hat{\eta}|\hat{k}_0)$ is found, $\{\hat{\eta}\}$ is readily computed by using the inverse method of generating random deviates [*Abramowitz and Stegun,* 1965].

The surface normal probability $P(\hat{\eta}|\hat{k}_0)$ is derived by first finding the conditional probability $P(\hat{k}_0|\hat{\eta})$ that $\hat{k}_0$ intersects dS, given the condition that the normal to dS lies between $\hat{\eta}$ and $\hat{\eta} + d\hat{\eta}$. This probability of intersection is taken to be

$$P(\hat{k}_0|\hat{\eta}) = \Lambda(\hat{k}_0, \hat{\eta})\Upsilon(\hat{k}_0, \hat{\eta}) \quad \text{(A1)}$$

where $\Lambda(\hat{k}_0, \hat{\eta})$ is the shadowing probability that a remote portion of the surface does not shadow dS from $\hat{k}_0$ and $\Upsilon(\hat{k}_0, \hat{\eta})$ is the normalized exposed area of dS defined as the ratio of the area of dS normal to $\hat{k}_0$ to the area of the entire mean surface normal to $\hat{k}_0$:

$$\Upsilon(\hat{k}_0, \hat{\eta}) = (\hat{k}_0\cdot\hat{\eta})\, dA/[(\hat{k}_0\cdot\hat{z})(\hat{\eta}\cdot\hat{z})A] \quad \text{(A2)}$$

where $\hat{z}$ is the unit normal to the mean surface, dA is the differential area of the projection of dS onto the mean surface, and A is the area of the entire mean surface. Parameter $\Upsilon(\hat{k}_0, \hat{\eta})$ accounts for the fact that an element dS normal to $\hat{k}_0$ is more likely to be intersected than an element that has the same area but is oblique to $\hat{k}_0$. The assumption is made [*Smith,* 1967] that shadowing is independent of $\hat{\eta}$ except through the unit step function $h(-\hat{k}_0\cdot\hat{\eta})$, which accounts for the situation in which the angle between $\hat{\eta}$ and $-\hat{k}_0$ exceeds $\pi/2$, totally ruling out the possibility of intersection. The shadowing probability is then given by

$$\Lambda(\hat{k}_0, \hat{\eta}) = \chi(\hat{k}_0)h(-\hat{k}_0\cdot\hat{\eta}) \quad \text{(A3)}$$

where $\chi(\hat{k}_0)$ is independent of $\hat{\eta}$.

The shadowing function $\chi(\hat{k}_0)$ can be evaluated by considering the probability $P(\hat{k}_0)$ that $\hat{k}_0$ intersects dS independent of conditions on $\hat{\eta}$:

$$P(\hat{k}_0) = \int d\eta_1 \int d\eta_2 P(\hat{k}_0|\hat{\eta})P(\hat{\eta}) \quad \text{(A4)}$$

where the region of integration is $\eta_1^2 + \eta_2^2 \le 1$ and $P(\hat{\eta})$ is the surface normal probability density function. $P(\hat{\eta})$ can be expressed in terms of $P(Z_u, Z_c)$, the probability density function of the upwind and crosswind large-scale slopes denoted by Z_u and Z_c. $P(Z_u, Z_c)$ is assumed to be a Gaussian distribution [*Cox and Munk,* 1954]:

$$P(Z_u, Z_c) = (2\pi\sigma_u\sigma_c)^{-1} \exp[-(Z_u^2/2\sigma_u^2) - (Z_c^2/2\sigma_c^2)] \quad \text{(A5)}$$

where σ_u and σ_c are the upwind and crosswind rms slopes. The relationships between Z_u, Z_c, and $\hat{\eta}$ are

$$Z_u = -\hat{\eta}\cdot\hat{u}/\hat{\eta}\cdot\hat{z} \quad \text{(A6)}$$

$$Z_c = -\hat{\eta}\cdot\hat{z}\times\hat{u}/\hat{\eta}\cdot\hat{z} \quad \text{(A7)}$$

where $\hat{u}$ is the unit vector in the upwind direction. Using (A6) and (A7), one obtains

$$P(\hat{\eta}) = P(Z_u, Z_c)/[(1 - \eta_1^2 - \eta_2^2)^{1/2}(\hat{\eta}\cdot\hat{z})^3] \quad \text{(A8)}$$

where the denominator is the Jacobian relating the Z_u, Z_c coordinates to the η_1, η_2 coordinates. The probability that $\hat{k}_0$ intersects any portion of the large-scale surface is given by the integral of $P(\hat{k}_0)$ over the entire mean surface A. Setting this integral equal to unity and solving for $\chi(\hat{k}_0)$ give

$$\chi(\hat{k}_0) = 2\pi^{1/2}/[-V^{-1}\exp(-V^2) + \pi^{1/2}\operatorname{erfc} V] \quad \text{(A9)}$$

where erfc denotes the complementary error function and

$$V = \hat{k}_0\cdot\hat{z}/\{2[(\hat{k}_0\times\hat{z})\cdot(\hat{k}_0\times\hat{z})\sigma_u^2 + (\sigma_c^2 - \sigma_u^2)(\hat{u}\cdot\hat{k}_0\times\hat{z})^2]\}^{1/2} \quad \text{(A10)}$$

The algebra of conditional probabilities gives the conditional surface normal probability density function:

$$P(\hat{\eta}|\hat{k}_0) = P(\hat{k}_0|\hat{\eta})P(\hat{\eta})/P(\hat{k}_0) \quad \text{(A11)}$$

APPENDIX B: SMALL-SCALE SCATTERING

The small-scale surface is assumed to be slightly rough, such that $k\zeta \ll 1$. The roughness is assumed to be isotropic and is specified by the small-scale sea spectrum $W_s(K)$. The normal to the surface's mean plane is denoted by $\hat{\eta}$. The incident radiation is a plane wave with propagation vector $\hat{k}_0$ and electric field $\hat{E}_0$ having unit magnitude. The incident field produces an incoherent scattered field and a coherent reflected field. Small-scale perturbation theory [*Rice,* 1951] represents the scattered field by a set of scattered plane waves. The magnitude of the scattered field $\mathbf{E}_s$ associated with one such plane wave having a unit propagation vector $\hat{k}_s$ is given by

$$|\mathbf{E}_s| = |(\hat{E}_0\cdot\hat{H}_0)(\beta_{hh}\hat{H}_s + \beta_{hv}\hat{V}_s) + (\hat{E}_0\cdot\hat{V}_0)(\beta_{vh}\hat{H}_s + \beta_{vv}\hat{V}_s)| \quad \text{(B1)}$$

where $\hat{H}_0$, $\hat{H}_s$, $\hat{V}_0$, and $\hat{V}_s$ are the horizontal and vertical polarization vectors for the incident and scattered radiation, with respect to normal $\hat{\eta}$:

$$\hat{H}_0 = (\hat{k}_0\times\hat{\eta})/|\hat{k}_0\times\hat{\eta}| \quad \text{(B2)}$$

$$\hat{V}_0 = \hat{k}_0\times\hat{H}_0 \quad \text{(B3)}$$

$\hat{H}_s$ and $\hat{V}_s$ are given by (B2) and (B3) with subscript s replacing $_0$. *Peake and Barrick* [1967] derived the scattering terms β_{mn}, $m = h$ or v and $n = h$ or v, to first order in $k\zeta$ to be

$$\beta_{mn} = 2k(-\hat{k}_0\cdot\hat{\eta})\alpha_{nm}N(K) \quad \text{(B4)}$$

where $N(K)$ is the roughness spectral coefficient and α_{nm} are the bistatic scattering matrix elements. These elements are functions of the surface permittivity ϵ and the angles Θ_0, Θ_s, and Φ_s, where Θ_0 is the angle made by $-\hat{k}_0$ and $\hat{\eta}$, Θ_s is the angle made by $\hat{k}_s$ and $\hat{\eta}$, and Φ_s is the angle made by the projections of $\hat{k}_0$ and $\hat{k}_s$ onto the mean plane of the surface. The radial wave number K of the spectral coefficient is given by

$$K = k\{|\hat{k}_s - \hat{k}_0|^2 - [(\hat{k}_s - \hat{k}_0)\cdot\hat{\eta}]^2\}^{1/2} \qquad \text{(B5)}$$

If a random rough surface as defined by *Rice* [1951] is assumed, the spectral coefficients have the property that

$$\langle|N(K)|^2\rangle = (\pi/L)^2 W_s(K) \qquad \text{(B6)}$$

where L^2 is the area of the mean scattering surface and angle brackets denote the average over the ensemble of surfaces. The number of scattered plane waves in a solid angle $d\Omega_s$ in the direction of $\hat{k}_s$ is [*Peake and Barrick*, 1967]

$$dn = d\Omega_s(\hat{k}_s\cdot\hat{\eta})(kL/2\pi)^2 \qquad \text{(B7)}$$

The scattered power within $d\Omega_s$ is the power of the plane wave $\hat{k}_s$ multiplied by the number dn of plane waves in $d\Omega_s$. The power scattered between Θ_s and $\Theta_s + d\Theta_s$ divided by the incident power is given by $\gamma(\Theta_s, \hat{k}_0, \hat{\eta}) \sin\Theta_s\, d\Theta_s$, where $\gamma(\Theta_s, \hat{k}_0, \hat{\eta})$ is the small-scale zenith scattering coefficient that can be derived from the above equations:

$$\gamma(\Theta_s, \hat{k}_0, \hat{\eta}) = k^4(-\hat{k}_0\cdot\hat{\eta})(|\hat{E}_0\cdot\hat{H}_0|^2 I_h + |\hat{E}_0\cdot\hat{V}_0|^2 I_v)\cos^2\Theta_s \qquad \text{(B8)}$$

$$I_m = \int_{-\pi}^{\pi} d\Phi_s(|\alpha_{hm}|^2 + |\alpha_{vm}|^2)W_s(K) \qquad \text{(B9)}$$

where $m = h$ or v. The small-scale zenith scattering coefficient in terms of θ_s, the angle made by $\hat{k}_s$, and the normal $\hat{z}$ to the mean two-scale surface is approximated by (B8), θ_s replacing Θ_s. The emissivity, which is found by integrating (B8) over the zenith scattering angle, is not affected by this change in the integration variable.

The propagation vector $\hat{k}_r$ of the reflected radiation is given by

$$\hat{k}_r = \hat{k}_0 - 2(\hat{k}_0\cdot\hat{\eta})\hat{\eta} \qquad \text{(B10)}$$

The magnitude of the reflected field $\mathbf{E}_r$ is given by

$$|\mathbf{E}_r| = |(\hat{E}_0\cdot\hat{H}_0)R_h\hat{H}_r + (\hat{E}_0\cdot\hat{V}_0)R_v\hat{V}_r| \qquad \text{(B11)}$$

where $\hat{H}_r$ and $\hat{V}_r$ are the horizontal and vertical polarization vectors for the reflected radiation and are given by (B2) and (B3), subscript r replacing $_0$. R_h and R_v are the horizontal and vertical reflection coefficients.

$$R_m = \rho_m(\Theta_0)(1 - Q_m) \qquad \text{(B12)}$$

$$Q_m = (k\cos\Theta_0/2)\int_{-\infty}^{\infty} du \int_{-\infty}^{\infty} dw \cdot W_s\{[(u - k\sin\Theta_0)^2 + w^2]^{1/2}\}F_m(u, w) \qquad \text{(B13)}$$

where $m = h$ or v, $\rho_m(\Theta_0)$ are the Fresnel reflection coefficients, and the functions $F_m(u, w)$ are given by *Wu and Fung* [1972]. The reflected power divided by the incident power equals the squared magnitude of $\mathbf{E}_r$:

$$|\mathbf{E}_r|^2 = |\hat{E}_0\cdot\hat{H}_0|^2|R_h|^2 + |\hat{E}_0\cdot\hat{V}_0|^2|R_v|^2 \qquad \text{(B14)}$$

Q_m is of order $(k\zeta)^2$. Keeping only terms of order $(k\zeta)^2$ or less gives

$$|R_m|^2 = |\rho_m(\Theta_0)|^2(1 - 2\,\mathrm{Re}\,Q_m) \qquad \text{(B15)}$$

where Re denotes the real part and $m = h$ or v.

When the surface is a perfect conductor, energy conservation requires that the sum of the scattered power and the reflected power equals the incident power. Since the imaginary part of the permittivity ϵ goes to infinity for a perfect conductor, a statement of energy conservation is

$$\lim_{\mathrm{Im}\,\epsilon\to-\infty}\left[|\mathbf{E}_r|^2 + \int_0^{\pi/2} d\Theta_s \cdot\sin\Theta_s\gamma(\Theta_s, \hat{k}_0, \hat{\eta})\right] = 1 \qquad \text{(B16)}$$

The above limit is verified by *Wentz* [1974].

Acknowledgments. Much of this research was done at Radiometric Technology, Inc., Wakefield, Massachusetts, under a National Environmental Satellite Service contract 3-35345. I wish to thank A. E. Strong, E. P. McClain, and J. Alishouse of NOAA/NESS for their support. I am also grateful for information supplied by J. P. Hollinger of the Naval Research Laboratory and by R. A. Stacy and W. J. Pierson of the City University of New York.

REFERENCES

Abramowitz, M., and I. A. Stegun, *Handbook of Mathematical Functions*, p. 950, Dover, New York, 1965.

Allen, C. W., *Astrophysical Quantities*, p. 120, Oxford University Press, New York, 1963.

Cardone, V. J., Specification of the wind field distribution in the marine boundary layer for wave forecasting, *Rep. TR 69-1*, Geophys. Sci. Lab., New York Univ., New York, Dec. 1969.

Cox, C., and W. Munk, Measurement of the roughness of the sea surface from photographs of the sun's glitter, *J. Opt. Soc. Amer.*, *44*(11), 838–850, 1954.

Hollinger, J. P., Passive microwave measurements of the sea surface, *J. Geophys. Res.*, *75*(27), 5209–5213, 1970.

Hollinger, J. P., Passive microwave measurements of sea surface roughness, *IEEE Trans. Geosci. Electron.*, *9*(3), 165–169, 1971.

Peake, W. H., Interaction of electromagnetic waves with some natural surfaces, *IRE Trans. Antennas Propagat.*, *7*, spec. suppl., S324–S329, 1959.

Peake, W. H., and D. E. Barrick, Scattering from surfaces with different roughness scales: Analysis and interpretation, *Res. Rep. BAT-197A-10-3*, Battelle Mem. Inst., Columbus, Ohio, Nov. 1967.

Pierson, W. J., and R. A. Stacy, The elevation, slope and curvature spectra of a wind roughened sea surface, *Contract. Rep. NASA CR-2247*, Langley Res. Center, NASA, Hampton, Va., Dec. 1973.

Porter, R. A., and F. J. Wentz, Microwave radiometric study of ocean surface characteristics, *Contract. Rep. 135140*, Nat. Environ. Satell. Serv., NOAA, Washington, D. C., July 1971.

Rice, S. O., Reflection of electromagnetic waves from slightly rough surfaces, *Commun. Pure Appl. Math.*, *4*, 351–378, 1951.

Semyonov, B. I., Approximate computation of scattering of electromagnetic waves by rough surface contours, *Radio Eng. Electron Phys.*, *11*, 1179–1187, 1966.

Smith, B. G., Geometrical shadowing of a random rough surface, *IEEE Trans. Antennas Propagat.*, *15*(5), 668–671, 1967.

Stogryn, A., The apparent temperature of the sea at microwave frequencies, *IEEE Trans. Antennas Propagat.*, *15*(2), 278–286, 1967.

Strong, A. E., Mapping sea surface roughness using microwave radiometry, *J. Geophys. Res.*, *76*(36), 8641–8648, 1971.

Van Melle, M. J., H. H. Wang, and W. F. Hall, Microwave radiometric observations of simulated sea surface conditions, *J. Geophys. Res.*, *78*(6), 969–976, 1973.

Wentz, F. J., The effect of surface roughness on microwave sea brightness temperatures, *Contract. Rep. 3-35345*, Nat. Environ. Satell. Serv., NOAA, Washington, D. C., March 1974.

Wu, S. T., and A. K. Fung, A noncoherent model for microwave emissions and backscattering from the sea surface, *J. Geophys. Res.*, *77*(30), 5917–5929, 1972.

(Received October 29, 1974;
accepted March 6, 1975.)